# Electroactive Bi-Functional Liquid Crystal Elastomer Actuators

Gaoyu Liu, Yakui Deng, Bin Ni, Giao Nguyen, Cédric Vancaeyzeele, Annie Brûlet, Cédric Plesse, Min-Hui Li, Frédéric Vidal

# Electroactive Bi-functional Liquid Crystal Elastomer Actuators

*Gaoyu Liu,[1#] Yakui Deng,[1#] Bin Ni,[1] Giao T. M. Nguyen,[2] Cédric Vancaeyzeele,[2] Annie Brûlet,[3] Frédéric Vidal,[2] and Cédric Plesse,[2,*] Min-Hui Li[1,*]*

[1] Chimie ParisTech, Université Paris Sciences & Lettres, CNRS, Institut de Recherche de Chimie Paris, UMR8247, 11 rue Pierre et Marie Curie, 75005 Paris, France

[2] CY Cergy Paris Université, Laboratoire de physicochimie des polymères et des interfaces (LPPI), 5 mail Gay Lussac, 95031 Cergy-Pontoise Cedex, France

[3] Laboratoire Léon Brillouin, Université Paris-Saclay, UMR12 CEA-CNRS, CEA Saclay, 3 rue Joliot Curie, 91191 Gif sur Yvette cedex, France

* E-mail: min-hui.li@chimieparistech.psl.eu; cedric.plesse@cyu.fr

# These authors contributed equally.

Keywords: liquid crystal elastomer (LCE), electroactive actuator, bending, contraction, conducting polymer

Liquid crystal elastomers (LCEs) with promising applications in the field of actuators and soft robotics have been reported. However, most of them are activated by external heating or light illumination. The examples of electroactive LCEs are still limited; moreover, they are monofunctional with one type of deformation (bending or contraction). We report here on a trilayer electroactive LCE (eLCE) by intimate combination of LCE and ionic electroactive polymer device (i-EAD). This eLCE is bi-functional and can perform either bending or contractile deformations by the control of the low-voltage stimulation. By applying a voltage of ±2 V at 0.1 Hz, the redox behavior and associated ionic motion provide a bending strain difference of 0.80%. Besides, by applying a voltage of ±6 V at 10 Hz, the ionic current-induced Joule heating triggers the muscle-like linear contraction with 20% strain for eLCE without load. With load eLCE can lift a weight of 270 times of eLCE-actuator weight, while keeping 20%

strain and affording 5.38 kJ·m$^{-3}$ work capacity. This approach of combining two smart polymer technologies (LCE and i-EAD) in a single device is promising for the development of smart materials with multiple degrees of freedom in soft robotics, electronic devices, and sensors.

## 1. Introduction

In the last decades, the stimuli-responsive smart materials that actively undergoes a predetermined change in their geometry or dimensions upon external stimulations are the focus of the research of many scientists and engineers.[1] Among them, liquid crystal elastomers (LCEs), especially the uniformly ordered nematic LCEs, possess fascinating features combining the entropic elasticity of elastomers and the ability to undergo a reversible and alignment-dependent shape-change behavior of liquid crystal polymers (LCPs).[2-7] Thus, LCEs show promising potentials as smart actuators, for example, those contracting/expanding linearly like mammalian muscles.[8] LCEs are thermo-active because they are based on thermotropic liquid crystals.[9-12] When photo-responsive units like azobenzene are incorporated in the LCE chemical structures, LCEs exhibit photo-mechanical properties.[13-21] Accordingly, temperature and light are the most used stimuli in actuators and sensors made of LCEs. However, in the world of actuators, electrical energy is the most convenient and the most in demand stimuli. Indeed, the nature does use electrical impulses between nerves and muscles/skins for actuation and sensing with extraordinary efficacy, and electrical stimulation is also more widely utilizable as driving forces in industrial devices. Efforts have been made to achieve electroactive LCEs (eLCEs). The first example of eLCE is made of ferroelectric smectic LCE film of a thickness of 100 nm, where 4% strain has been achieved under an electric field of 1.5 MV m$^{-1}$ by electroclinic effect of ferroelectric LC.[22] Then, most of eLCEs were electrothermal systems developed from nematic LCEs by introducing Joule effect,[23-38] or Peltier effect[39]. These eLCEs achieved the strain (typically 10%-100%) and stress of normal nematic LCEs via

electrothermal effect under low voltage (typically < $10^2$ V). The most studied electrothermal nematic eLCEs use Joule heating and can be divided into two categories, one is electronic eLCEs where the Joule effect is introduced by highly conducting materials like graphite,[23] carbon black,[24,25] carbon nanotubes,[26] metal wires,[27-30] liquid metals[31-33]; another one is ionic eLCEs where LCE is combined with ionic electroactive polymer device (i-EAD)[34-38].

The i-EAD is also an interesting smart material by itself due to its low driving voltage (in the range of few volts) and the ability to operate in open-air and to convert either electrical stimulation into reversible large bending deformations (actuator) or mechanical stimulation into electrical signal (sensor). Typical tri-layer i-EAD[40-42] consists of an ionic conducting membrane sandwiched by two electronically conducting polymers (ECPs) as electrodes; the most popular ECP is poly(3,4-ethylenedioxythiophene) doped with polystyrene sulfonate (PEDOT-PSS).[43-47] Indeed, upon electrical stimulation at low voltage and low frequency, ECP can be electrochemically oxidized or reduced in the presence of an electrolyte. To insure the overall electroneutrality of ECP, the expulsion or insertion of ions takes place within the ECP, leading to the shrinkage or swelling of the ECP layer. With the tri-layer configuration, the opposite volume variations occurring at the cathode and the anode result in a large bending movement of the i-EAD. However, large muscle-like linear contraction/elongation is sparsely reported for this type of i-EAD, and the few examples exhibited low strokes (only about 0.5% contraction ratio).[41,48] Therefore, the development of ionic eLCEs, by implementing the electrical stimulus and achieving large muscle-like linear contractions appears clearly as a promising approach to develop multifunctional smart materials with unprecedented behaviours and motions.

Nevertheless, a few tentative works in this direction[34-38] only showed limited effects. Domenici *et al*.[34,35] proposed a bi-layer system, where a conductive PEDOT:PSS thin layer was deposited on the surface of a well-aligned (monodomain) nematic LCE. They only observed bending or microwinkling deformation under electrical stimuli. Jakli *et al*.[36,37] used a tri-layer system,

where a nematic LCE membrane containing ionic liquids was sandwiched by two conductive PEDOT:PSS thin layer. Again, only bending deformation was observed under electrical stimuli, though an improvement in electroactive bending of i-EAD was obtained by the LC alignment. Other reports of LCEs containing ionic liquids[37,38] just showed increased performance of mechanoelectrical response in sensing mode. In brief, no electroactive linear actuation was achieved in the reported systems,[34-38] probably because the change of conformation of LC polymer chain was not obtained by the electronical stimulation.

In this paper, we report on the first system of bi-functional ionic eLCEs that can perform both bending deformation and linear contraction/elongation, all under the control of electrical signals (Figure 1). A tri-layer system composed of carefully designed ionically conducting LCE membrane sandwiched between two layers of PEDOT:PSS has been adopted in our ionic eLCEs. By applying a low voltage at low frequency, the redox behavior and associated ionic motion of the i-EAD component provide bending deformation of the device. On the other hand, the application of a low voltage at higher frequency generates an ionic current-induced Joule heating that triggers the muscle-like contractile response of the eLCE membrane; linear contraction/elongation deformations of the device are finally achieved. This approach of combining two synergetic smart polymer technologies, i.e., LCEs and i-EAD, in a single device, is promising for the development of smart materials with multiple degrees of freedom, which are much sought after in the field of soft robotics.

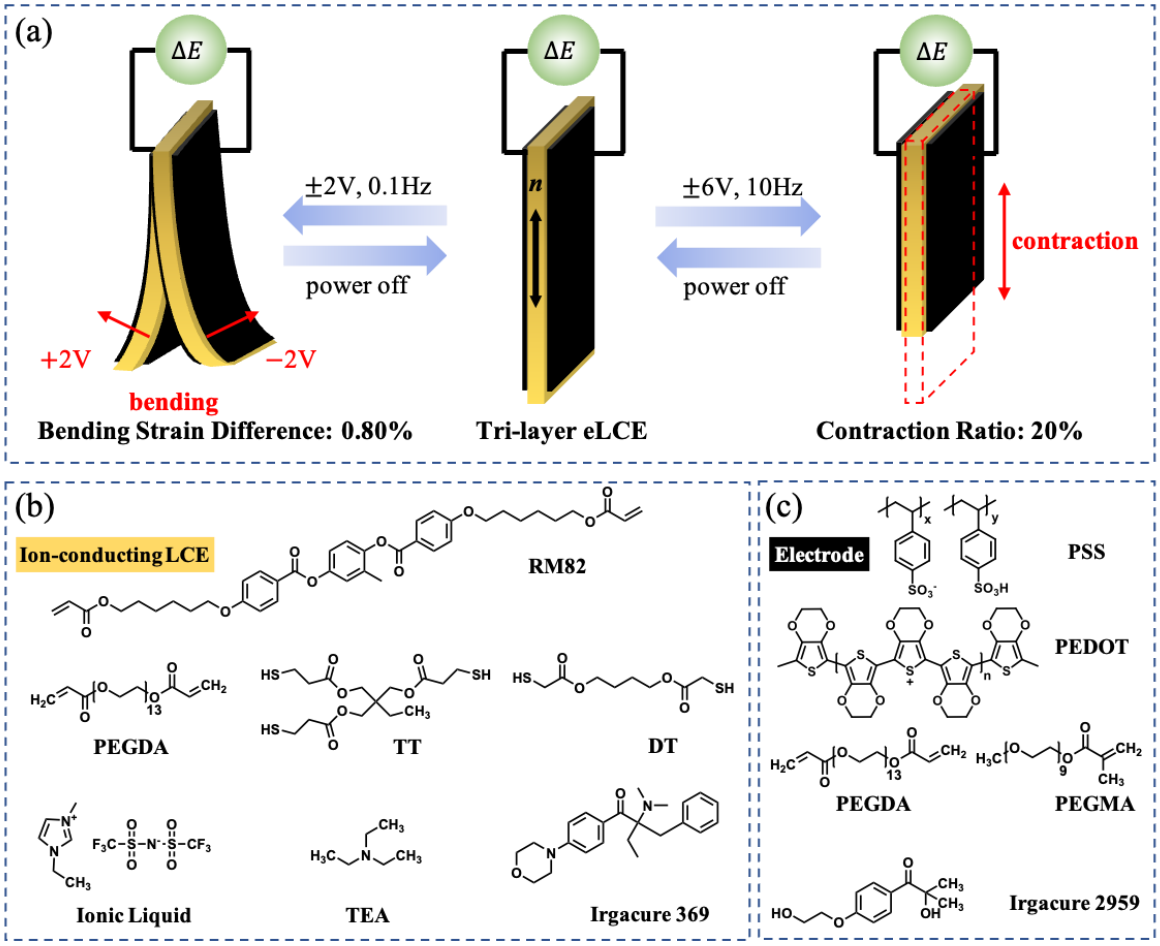


**Figure 1.** (a) Bi-functional trilayer eLCE film: the yellow central layer represents the ionically conducting LCE film (***n*** indicating the nematic alignment direction) and the two black side layers represent the PEDOT:PSS-based ECP electrodes. The trilayer eLCE performs both bending deformation (±2 V, 0.1 Hz, bending strain: 0.80%) and linear contraction/elongation deformation (±6 V, 10 Hz, contraction ratio: 20%). (b) Chemical structures of the components to make central LCE film. (c) Chemical structures of the components to make the PEDOT:PSS electrodes.

## 2. Results and Discussion

### 2.1. Ion conducting LCE membrane: preparation and characterization

Figure 1a shows the trilayer ionic eLCE composed of an ion conducting LCE membrane in the center and two PEDOT:PSS-based ECP electrodes attached to the both surfaces of LCE membrane. The central LCE membrane was first prepared by a two-stage

polymerization/crosslinking[12] of the LC monomer RM82 in the presence of an ionic liquid. The complete composition of LCE membrane is shown in Figure 1b and its preparation in Scheme S1 in supporting information (SI) (also see SI for detailed preparation procedure). The RM82 is a commercially available LC monomer and chosen because of its relatively low nematic to isotropic phase transition temperature ($T_{NI}$ = 65 °C).[36] Poly(ethylene glycol)diacrylate (PEGDA) was used as co-monomer of RM82 due to its affinity with the ionic liquid electrolyte chosen here, 1-ethyl-3-methylimidazolium bis(trifluoromethylsulfonyl)imide (EMIM TFSI). 1,4-butanediol bis(thioglycolate) (DT), trimethylolpropane tris(3-mercoptopropianate) (TT) and triethylamine (TEA) were chain extender, crosslinker and base catalyst, respectively, in the first stage polymerization/crosslinking by thiol-acrylate Michael addition click reaction. The total acrylate groups and thiol groups are not equimolar; the acrylates were in excess so that the second polymerization/crosslinking based on acrylate would be carried out later. A slightly crosslinked polydomain LCE was obtained after the thiol-acrylate Michael addition, where mesogens aligned in the same direction only in local domains and the director of each domain (***n***) was random. Then, a mechanical stretch of this polydomain LCE was performed to get mesogens orientated uniformly along the stretching direction. Finally, a second polymerization/crosslinking through free radical thiol-ene addition of remaining thiol groups of the first stage and free radical polymerization of acrylates leftover was conducted under UV light in the presence of Irgacure 369, to complete the network formation and lock the LC orientation. A moderately crosslinked monodomain LCE was thus obtained, which features global alignment and shows large anisotropy in various macroscopic properties.

The key components in the ionically conducting LCE membrane are LC monomer RM82 and PEG-containing monomer PEGDA, because the linear actuation depends on the LC part, while the part from PEGDA has affinity with ionic liquid to ensure the ionic mobility. The balance between these two components is of paramount importance for the performance of LCE membrane. Therefore, a series of LCE films (named as LCE1, LCE2, LCE3, LCE4 and LCE5)

with the molar ratio RM82:PEGDA = 6:1, 4:1, 2:1, 1:1 and 1:4, respectively, have been prepared (see Table S1 and synthetical detail in SI). All these films have been carefully characterized. The polymer network formation was confirmed using Fourier transform infrared (FT-IR) spectroscopy by observing the disappearance of acrylate C=C band at 1623 $cm^{-1}$ in final aligned LCE (Figure S1).

To find the optimal molar ratio of RM82:PEGDA for ion conducting LCE, both contraction/elongation deformation and ionic conductivity of these films have been evaluated. Figure 2a and Figures S2-4 show thermal responsive contraction and elongation of the samples LCE1-5 upon heating-cooling cycle. The contraction ratio is defined as $(L_0 - L)/L_0$, where $L_0$ is the original length of the film at 25 °C and $L$ the film length at any given temperature. The maximal contraction ratio at T = 100 °C after nematic-isotropic transition was measured as 28%, 24% and 10% for LCE1, LCE2 and LCE3, respectively. As expected, the contraction ratio decreases with the RM82 molar ratio's decreasing, until no contraction for LCE4 and LCE5 with the molar ratio RM82:PEGDA equal to or below 1:1. Then, polarized optical microscopy (POM) and two-dimensional wide angle X-ray scattering (2D-WAXS) were employed to examine the sample orientation. The light transmission of the sample LCE1, 2 or 3 placed with alignment direction (***n***) parallel to polarizer (p) was clearly different from the sample placed with ***n*** tilted at 45° relative to p (Figure 2b and Figure S2-S4). 2D-WAXS allowed to quantify the alignment and its evolution as a function of temperature as shown in Figure 2c for LCE2 (see Figure S5 for more patterns at room temperature and Video S1 for patterns of LCE2 upon heating and cooling). The nematic order parameter S was calculated from the angular profile of crescent-like signals along the alignment direction[49] (see SI for details). For example, for LCE2 S = 0.48 at 25 °C (nematic), while S = 0.18 at 130 °C (isotropic). The order parameter S as a function of temperature (Figure S6) exhibits a crossover located around 80 °C that corresponds to the nematic-isotropic transition ($T_{NI}$). However, some anisotropic order still existed after $T_{NI}$ at high temperature even after the film shrunk completely. This observation

can be explained by the crosslinked nature of the material that may prevent full relaxation toward the complete disordered state. As expected, the order parameter at 25 °C decreased with the nematic molecule (RM82) molar proportion, with S = 0.54 ± 0.2 for LCE1, S = 0.48 ± 0.2 for LCE2, S = 0.35 ± 0.2 for LCE3 and S = 0.33 ± 0.2 for LCE4 (see Figure S5). This result is coherent with the tendency of the decrease of contraction ratio. In conclusion, from the point of view of contraction/elongation performance, LCE1, LCE2 and LCE3 with contraction ratio of 28%, 24% and 10%, respectively, are the valuable candidates for the construction of ionic eLCEs.

Then, ionic conductivity ($\sigma$) of LCE1, LCE2 and LCE3 were measured by electrochemical impendence spectroscopy (EIS) in the temperature range of 20-70 °C (see SI for detail).[50] At 20 °C, $\sigma$ (LCE1) was measured as $5.3\times10^{-5}$ S/cm , $\sigma$ (LCE2) as $1.0\times10^{-4}$ S/cm and $\sigma$ (LCE3) as $4.2\times10^{-4}$ S/cm. As expected, the $\sigma$ value increased with the increase of polar component PEGDA. The ionic conductivity was also improved upon heating as shown in Figure 2d. At 70 °C, $\sigma$ (LCE1) was measured as $4.0\times10^{-4}$ S/cm, $\sigma$ (LCE2) as $4.4\times10^{-4}$ S/cm and $\sigma$ (LCE3) as $2.2\times10^{-3}$ S/cm. The small angle X-ray scattering (SAXS) experiment on LCE2 effectively showed the phase segregation between LC-rich domains and PEG-rich domains, where the PEG-rich domains ensure the ionic conduction (see Figure S7-S9 in SI for data and discussion). Analysing both contraction/elongation deformation and ionic conductivity of LCE1, 2 and 3 films, LCE2 showed a good balance of these two properties: linear contraction ratio of 24% that is close to the value of natural muscle, and the ionic conductivity $\sigma$ at the order of $10^{-4}$ S/cm that is a reasonable value for electroactive LCE.[36,38] Therefore, LCE2 was selected as the central membrane of trilayer ionic eLCEs, and further thermal mechanical characterization was made on LCE2.

The thermal stability of LCE2 was first examined by thermogravimetric analysis (TGA) (see Figure S10), showing degradation onset temperature with 5% of mass loss ($T_{5\%}$) of 330 °C and

thus a good thermal stability. The quasi-static stress-strain curve of LCE2 film at 25 °C was measured using the universal tensile machine by stretching the films along the nematic orientation direction. The Young's modulus and breaking strength of LCE2 film reached 1.22 MPa and 0.84 MPa, respectively (Figure S11). The thermal mechanical properties of LCE2 were then studied by dynamic mechanical analysis (DMA). Figure 2e shows the typical viscoelastic behavior of the film at temperature ramp mode. The α relaxation temperature ($T_\alpha$) of LCE2 is -4.8 °C corresponding to the loss factor tan δ peak. The storage modulus E' decreased upon heating and tended to a rubbery plateau at T > 25 °C. However, a careful analysis on the E' curve of LCE2 revealed a slightly re-increasing tendency of E' after T = 80 °C (indicated by the black vertical dotted line) that corresponds to the nematic-isotropic phase transition ($T_{NI}$, see WAXS results above-discussed and Figure S6). This re-increasing tendency of E' was attributed to the contraction deformation occurred at $T_{NI}$. To confirm this assignment, a heating-cooling-heating cycle with supplemental heating run was performed to check the reproducibility of this E' re-increasing tendency. If it was not reproducible, it could be attributed to an irreversible secondary crosslinking at high temperature. Figure S12 effectively shows the reproducibility of this E' re-increasing tendency and confirmed its origin of LCE thermal contraction at nematic-isotropic transition. To evaluate the LCE thermal actuating behavior, LCE2 film was exposed to temperature ramps from 20 °C to 140 °C and from 140 °C to 20 °C ($T_{NI} \approx 80$ °C), and the deformation strain was measured in iso-stress mode (stress = 0.02 N) by DMA. The obtained strain curves as a function of time are presented in Figure 2f. Reversible strains from 0% to −33% during the heating-cooling cycle indicate the LCE2 film contracts and elongates reversibly with sweeping temperature. All above thermal mechanical characterizations confirm the thermal actuation performance of LCE despite the presence of the ionic liquid EMIM TFSI. Moreover, for comparison the pure LCE without ionic liquids was also prepared by the same two-stage polymerization/crosslinking method. This pure LCE film was tested by DMA at iso-stress mode. Figure S13 shows the slope of strain *vs* time

(0.07% $S^{-1}$) of both LCE2 without and with ionic liquids (Figure S13a-b) are nearly the same. However, the maximum reversible strain was 45% for the LCE2 without ionic liquids during the heating-cooling cycle, while it was 33% for the LCE2 with ionic liquids. Therefore, the existence of ionic liquids does not affect the thermal actuation speed but affects the contraction ratio of LCE due to their dilution effect in the LCE sample.

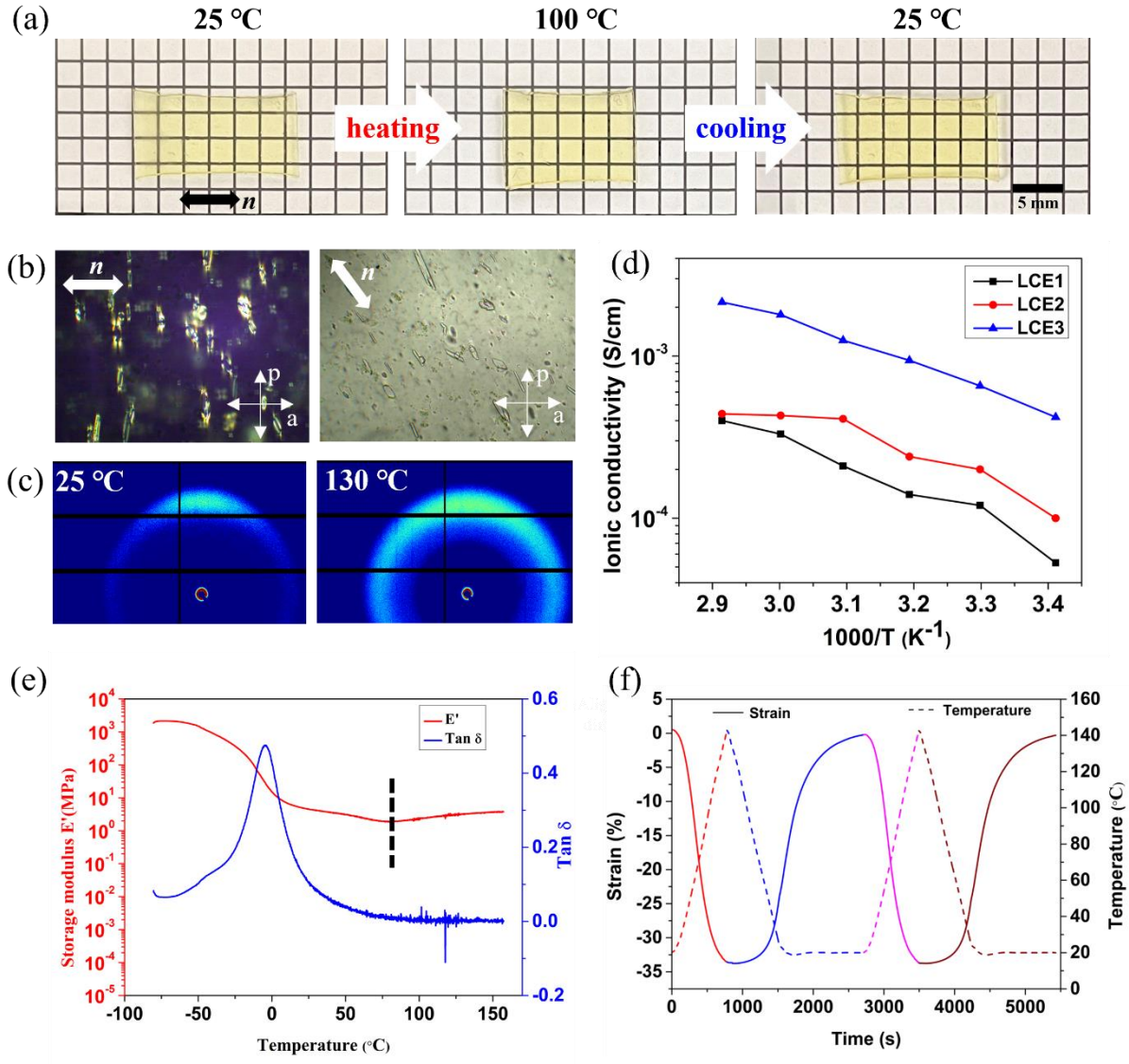


**Figure 2.** Characterization of the LCE2 film (RM82:PEGDA = 4:1). (a) Reversible contraction/elongation deformation upon heating and cooling. (b) Polarizing optical microscopic (POM) images with the alignment direction (***n***) either parallel (left) or tilt at angle θ = 45° (right) to the polarizer (p) (a indicating the analyzer). (c) 2D-WAXS (wide angle X rays scattering) patterns at 25 °C (nematic) and 130 °C (isotropic). (d) Ionic conductivity of LCE1,

LCE2 and LCE3 as a function of temperature. The abscissa is expressed in 1000/T with temperature in degree Kelvin. The measured temperature range is 20 -70 °C. (e) Storage modulus (E') and loss factor tan δ by DMA at temperature ramp mode (ramp rate: 3 °C/min, strain control: 0.05 %). (f) Deformation strain at iso-stress mode by DMA (ramp rate: ±3 °C/min, stress control: 0.02 N).

**2.2. Trilayer ionic eLCE**

The ionically conducting LCE membrane (LCE2) was then combined with PEDOT:PSS polymer electrodes (Figure 1c) for the preparation of trilayer ionic eLCE (see Scheme S2). PEDOT:PSS was chosen as ECP electrode due to its commercial availability, high conductivity, and ability to be casted directly on ionic membranes.[44] Into the pristine PEDOT:PSS, PEGDA and PEGMA bearing flexible short chains and dimethyl sulfoxide (DMSO) were added to improve the ionic mobility and electrical conductivity.[42] The photo-initiator Irgacure 2959 was also added in order to initiate polymerization/crosslinking of the (meth)acrylate end-groups of PEGDA and PEGMA to get electrode with better mechanical properties (such as elasticity). Concretely, PEDOT:PSS and additives were first deposited on the top surface of LCE2 followed by the water evaporation at 50 °C for 1 hour. The sample was let to return to room temperature and exposed to UV light for photo-polymerization/crosslinking to obtain the first electrode. Then, the sample was turned over and the procedure was repeated for the other surface of LCE2 to obtain the second electrode (see Scheme S2 and SI for elaboration procedure).[51] To measure the thickness of electrode, the same mixture of PEDOT:PSS electrode was deposited on a glass slide with the same area as the LCE2. The thickness of the PEDOT:PSS electrode was then measured accurately as 0.008 mm by profilometer DEKTAK 150. Its electronic conductivity ($\sigma_e$) was 319.14 S/cm (see SI for detail).[42]

The good thermal stability of the eLCE was assessed by TGA with degradation onset temperature $T_{5\%}$ at 280 °C (Figure S10). The deformation strain of trilayer eLCE in iso-stress mode was measured by DMA to verify if the eLCE kept the thermally induced linear actuation.

Figure S14 showed that during the first heating, 33% contraction strain was obtained. In the subsequent first cooling, the eLCE could recover 90% of its initial length. In the following heating/cooling cycle, the contraction/elongation is nearly reversible with deformation strain of 23%. The first 10% irreversible deformation is probably caused by the presence of PEDOT:PSS electrodes. Nevertheless, the PEDOT:PSS electrodes were globally compatible with the thermal contraction/elongation deformation of LCE. The electroactive redox process of the trilayer eLCE film was then analyzed by cyclic voltammetry (CV). As shown in Figure S15, CV curves indicated the occurrence of expected redox process in PEDOT:PSS electrodes within voltage scan between 3 V and -3 V,[52] with anodic peak and cathodic peak potentials $E_{pa}$ = 1.20 V and $E_{pc}$ = -1.10 V. Therefore, in the following electro-actuation studies, we start with the voltage of 2 V.

The electroactive bending deformation of the trilayer eLCE was first investigated under a square wave potential of ±2 V at different frequency from 0.0125 to 20 Hz. Figure 3a gives a schematic illustration of the principle of electroactive bending. When applying a positive potential on the top electrode (anode), the PEDOT in the electrode is oxidized to $PEDOT^{x+}$. As PSS acts as an ion selective layer, it allows only cation motion within PEDOT:PSS electrode. To keep charge neutrality, cations will be expelled from oxidized electrode leading to a shrinkage of the top electrode. On the bottom electrode (cathode), inverse phenomenon occurs; $PEDOT^{y+}$ in the electrode is reduced to PEDOT. To keep charge neutrality, cations will be inserted into the cathode causing its expansion. The top-shrinkage and bottom-expansion led finally to a bending deformation toward top side (Figure 3a).[40] When applying a negative potential on the top electrode (now cathode), an inverse bending deformation toward bottom side was obtained (see Figure 3b and also Video S2 for deformation movie). Figure 3b shows the photographic images of trilayer eLCE bending deformation under potential of ±2 V at 0.1 Hz. The precise mechanical bending responses were recorded by a laser displacement sensor (Figure 3c), and the bending deformation was quantified by the bending strain difference (Δε)

between the two electrodes (Figure 3d and see "electrochemomechanical characterizations" in SI ). As shown in Figure S16, for the trilayer eLCE under electrical stimulation of ±2 V the bending strain difference Δε of 1.3% was achieved at 0.0125 Hz, the lowest frequency tested. A value of Δε of 0.80% was obtained at 0.1 Hz (Figure 3e). The corresponding currents in the system were also measured as a function of time (Figure 3f). The value of Δε decreased rapidly with the increase of frequency with Δε of 0.14% at 1 Hz, and it became insignificant when the frequency was above 5 Hz. This result is expected since the bending actuation is based on ion diffusion that is slow by nature. Therefore, lower frequency (longer time) is favorable to reach higher strain difference Δε. On the other hand, the ionic conductivity of the central LCE membrane (a LC ionogel) remains limited ($10^{-4}$ S/cm) here, while ionic conductivities of ionogels can be increased above $10^{-3}$ S/cm with proper design.[53] Therefore, there is room for improvement with the bending strain in the future.

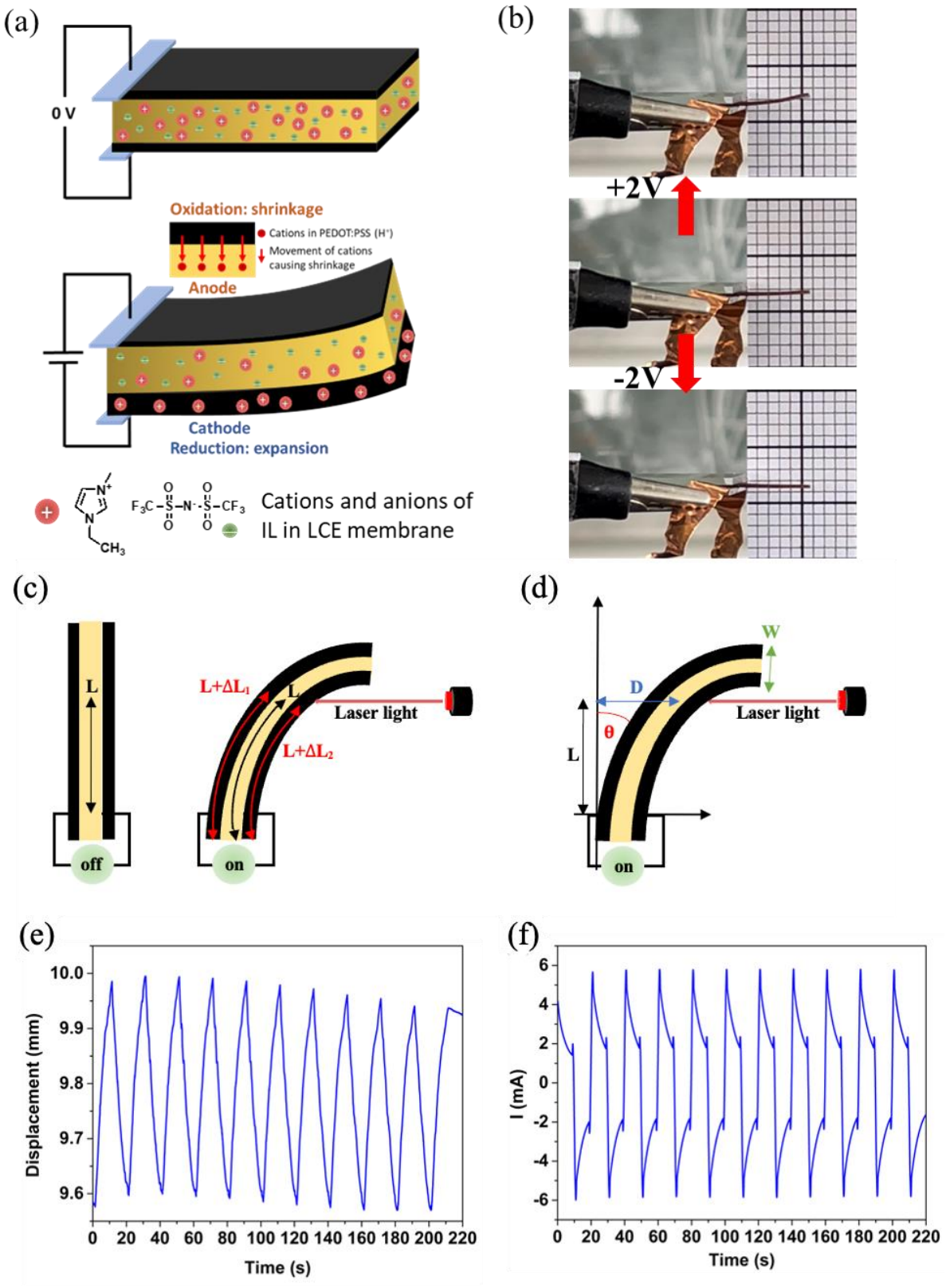


**Figure 3.** The mechanical response of trilayer eLCE (PEDOT:PSS)/LCE2/(PEDOT:PSS) (length: 16 mm, width: 6.5 mm, thickness: 0.5 mm) to electrical stimulation of square wave potential ±2 V at 0.1 Hz. (a) Schematic illustration of the principle of electroactive bending. (b)

Images of trilayer eLCE bending deformation (the background graphic paper with lines every 2 mm). (c) Schematic representation of the length changes of the two electrodes. (d) Illustration of the method to measure the bending strain difference $\Delta\varepsilon$ by a laser sensor. $\Delta\varepsilon = \Delta L/L = ((L+\Delta L_1) - (L+\Delta L_2))/L$, where L is the distance from the clamped end of the actuator to the projection point of the laser on the original sample, $(L+\Delta L_1)$ the length of the expending side, $(L+\Delta L_2)$ the length of contracting side, D the displacement, θ the bending angle and w the thickness of the actuator. (e) Displacement D recorded by the laser sensor as a function of time. The bending deformation with $\Delta\varepsilon = 0.80\%$ can be repeated at least 80 times (only 10 times shown here). (f) The corresponding currents measured upon bending deformation.

Since the bending deformation became insignificant when the frequency was above 5 Hz, the frequency of 10 Hz was then chosen to test the electroactive contraction deformation of trilayer eLCE without bending behavior. The alternating ionic current is susceptible to produce Joule effect due to the movement of ionic species in the eLCE device, which can heat the LCE until nematic to isotropic transition. Keeping the frequency constant at 10 Hz, the square potential of ±2 V, ±3 V, ±4 V, ±5 V and ±6 V were applied, respectively, for the contraction test of trilayer eLCE. The contraction was observed only with ±6 V in the time scale of 10 mins. It is comprehensible because the Joule heat is proportional to the voltage square, the conductivity, and the time. A minimal voltage is necessary for a certain conductivity value to increase the speed of ionic motion in the LCE membrane and to improve the Joule effect for heating.[54] A more elaborate test was then made by applying the field (±6 V, 10 Hz) on the trilayer eLCE film until 200 seconds, and meanwhile measuring the currents, temperatures, and contractions of the sample. Figure S17 shows the currents as a function of time, the maximum current being reached around 160 s. However, a maximum of 20% contraction was observed at about 100 seconds, while T = 134 °C was recorded by thermal camera. In order to avoid unnecessary overheat of the sample, a square wave potential of ±6 V at 10 Hz frequency with a duration of

around 100 s or until the maximal contraction was adopted in the following for a pristine trilayer eLCE film.

Figure 4 shows the eLCE sample deformations without load (Figure 4a) and with load (4.70 mN) (Figure 4b) under 3 cycles of power on/off, currents (Figure 4c) and contraction ratio (Figure 4d) as a function of time being measured together with temperatures of sample at starting and maximal contraction states. After each power-on of about 100 s, the sample was left power-off for 20 mins of pause to let it return to room temperature. A maximum of 20% contraction at 134 °C was recorded for the free film without load during the 1$^{st}$ cycle and a nearly complete recovery of its initial length was obtained after cooling down to 23 °C (Figure 4a). However, the maximum contraction ratio was decreased to 16% and 8% for the 2$^{nd}$ cycle and 3$^{rd}$ cycle. The power-on duration to reach the maximal contraction was 74 s, 93 s and 157 s for the 1$^{st}$, 2$^{nd}$ and 3$^{rd}$ cycle, respectively. For the 3$^{rd}$ cycle, the extension of power-on time didn't lead to more contraction. Moreover, during the 3$^{rd}$ power-on the maximal sample temperature stagnated at 42 °C, while the current didn't increase after 180 s power-on (Figure S18). This is probably caused by the drop of the conductivity of eLCE, which could be attributed to damage or delamination PEDOT:PSS layers.

Then, a load was attached to the trilayer eLCE film along the orientation (length) direction to examine the ability of eLCE to perform mechanical work under electrical field of ±6 V and 10 Hz (Figure 4b). The own weight of the mobile part of eLCE film (the part playing the role of actuator) is about 0.0175 g (taking density as 1 g·cm$^{-3}$), while the total load of the hung standard weight and the clamp is of 4.80 g. During the 1$^{st}$ power-on, the eLCE film could lift the weight of 4.80 g (274 times of the actuator weight) up to 2 mm height ($\Delta h$) (see also Video S3 in SI). The work done by the eLCE was $9.40\times10^{-5}$ J with a work capacity of 5.38 kJ·m$^{-3}$ (see SI for details). The eLCE mechanical properties under the electroactive stimulation (±6 V and 10 Hz) during three cycles are shown in Table S2. The eLCE lifted the load to a smaller height $\Delta h$, *i.e.*, 1.5 mm and 1 mm, respectively, for the 2$^{nd}$ and 3$^{rd}$ cycle. The contraction ratios of 20%, 15%

and 10% for the loaded eLCE during three cycles were similar to those for the unloaded free eLCE. The current and contraction ratio as a function of the time were also similar in both loaded and unloaded cases. The work and work capacity decreased also gradually from 1$^{st}$, 2$^{nd}$ to 3$^{rd}$ power cycle.

As far as we are aware, this is the first example of bi-functional electroactive LCE that can perform either bending or contractile deformation under low voltages of low or high frequency (comparison in Table S3). The contractile deformation of eLCE can be repeated 3 times with strain of 20% - 10% and lift up the load 274 times of the eLCE actuator weight. The bending deformation with typically 0.80% of bending strain difference can be repeated at least 80 times (10 times shown in Figure 3c) without fatigue. The performance of eLCE could be improved in the future by increasing its ionic conductivity and the connection between PEDOT:PSS layers and LCE layer. Moreover, decreasing the thickness of the ion conducting LCE film could also be a promising approach. First, it could significantly improve the bending strain difference and bending rate due to geometrical consideration and the decrease of ionic resistance. Secondly, it could also improve the contractile deformation rate of the eLCE by promoting much faster heating and accelerating the cooling of the device by heat dissipation.

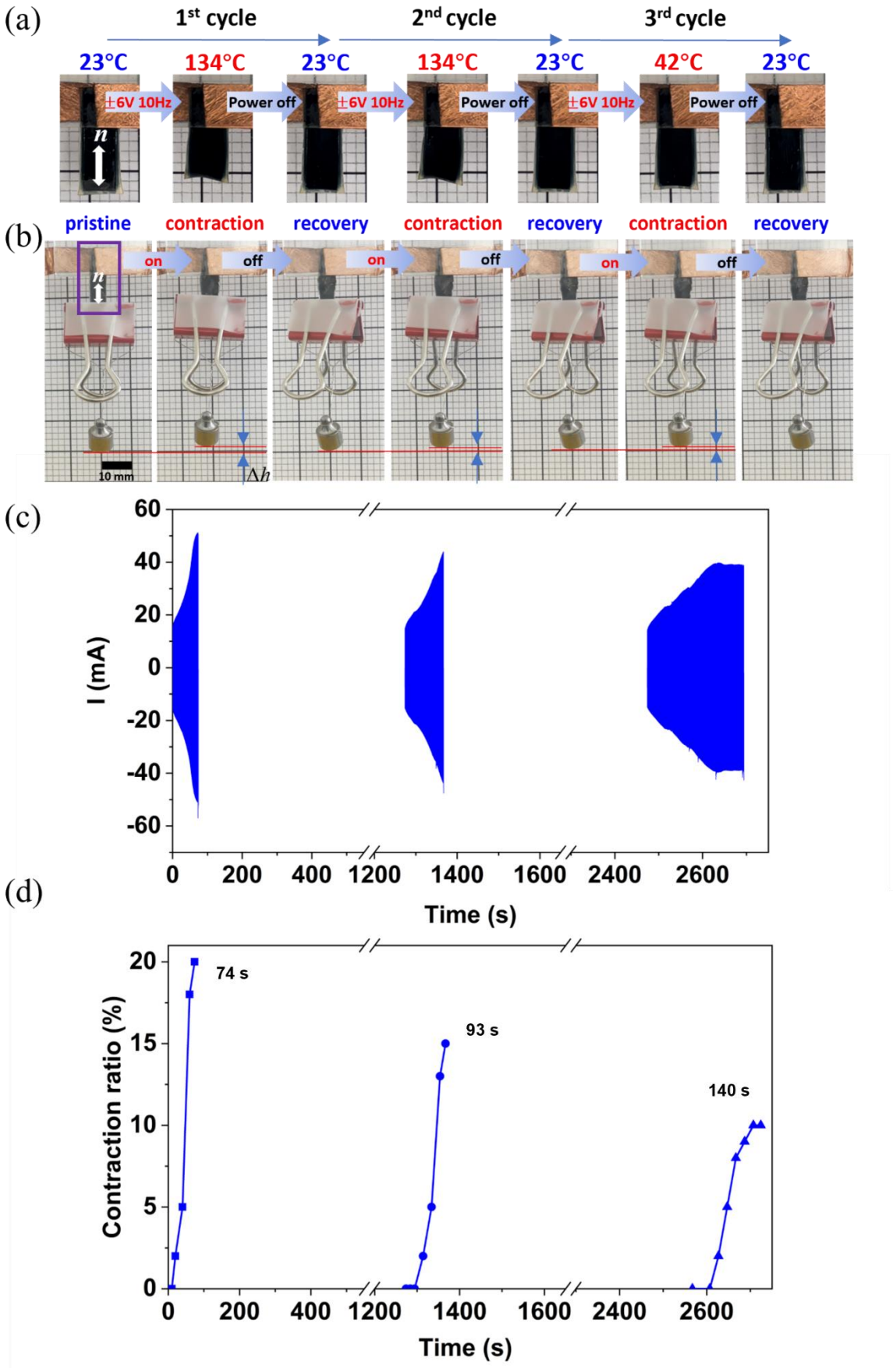
(a)
1st cycle
2nd cycle
3rd cycle
23°C
134°C
23°C
134°C
23°C
42°C
23°C
±6V 10Hz
Power off
±6V 10Hz
Power off
±6V 10Hz
Power off
n
(b)
pristine
contraction
recovery
contraction
recovery
contraction
recovery
on
off
on
off
on
off
n
10 mm
Δh
(c)
I (mA)
60
40
20
0
-20
-40
-60
0
200
400
1200
1400
1600
2400
2600
Time (s)
(d)
Contraction ratio (%)
20
15
10
5
0
74 s
93 s
140 s
0
200
400
1200
1400
1600
2400
2600
Time (s)

**Figure 4.** Linear electroactuations of trilayer eLCE film under square wave potential (±6 V, 10 Hz) during 3 power on/off cycles. (a) Images of trilayer eLCE films (black) without load. The top part of eLCE and two copper sheets (bronze) for electronical field connection are sandwiched between a pair of glass slides that is fixed to the sample holder. Only the mobile part of eLCE (length: 14 mm, width: 8 mm, thickness: 0.5 mm) is considered as actuator. Maximal contraction ratios of 20%, 16% and 8% are obtained for 1$^{st}$, 2$^{nd}$, and 3$^{rd}$ cycle of electroactivation, respectively. (b) Images of trilayer eLCE film (black, inside violet frame) with a load of 4.80 g. Only the mobile part of eLCE (length: 10 mm, width: 3.5 mm, thickness: 0.5 mm; 17.5 mg) is considered as actuator. The height of load lifting are $\Delta h$ = 2 mm, 1.5 mm, and 1 mm, respectively, for 1$^{st}$, 2$^{nd}$, and 3$^{rd}$ cycle of electroactivation. (c) Currents as a function of time during power-on of three cycles. (d) Contraction ratio as a function of time during power-on of three cycles. The maximal contractions were achieved after 74 s, 93 s and 140 s for the 1$^{st}$, 2$^{nd}$ and 3$^{rd}$ cycle, respectively.

## 3. Conclusion

In this work, we have elaborated eLCE actuators that can perform selectively either bending deformation or linear contractile deformation under electrical stimulation of low voltages, thanks to synergistic functionalities of ionic EAD and ion conducting LCE. The approach relied on the combination and interaction of two smart polymer technologies, i.e., LCEs and ionic EADs, in a single device made of an ion-conducting membrane based on aligned LC elastomers and two optimized conducting polymer electrodes as ionic EADs. By applying low voltage at low frequency (±2 V at 0.1 Hz), the redox behavior and associated ionic motion of the ionic EAD components provided bending deformation of eLCE up to a bending strain difference of 0.80%. On the other hand, by applying low voltage at higher frequency (±6 V and 10 Hz), the ionic current-induced Joule heating triggered the muscle-like contractile response of the ionically conducting LCE component, which made a linear contraction ratio of 20% of eLCE

without load and afford a work capacity of 5.38 $kJ \cdot m^{-3}$ with a load of 4.80 g (274 times of the weight of eLCE actuator) while keeping 20% strain. The possibility of this ionic eLCE actuator to perform simultaneously bending and contractile deformation is under investigation. Efforts are also being made to improve the anti-fatigue features of eLCE. The multifunctional ionic eLCE actuator developed here represents a promising approach to develop future smart materials with multiple biomimetic degrees of freedom like the emblematic octopus tentacle, long-time desired for soft robotics.

## Experimental Section/Methods

Experimental details are given in the Supporting Information.

## Supporting Information

Supporting Information is available from the Wiley Online Library or from the author.

## Acknowledgements

Gaoyu Liu and Yakui Deng contributed equally to this work. This work is financially supported by the French National Research Agency (ANR-22-CE06-0023, AS-LCE). The China Scholarship Council (CSC) is gratefully acknowledged by Gaoyu Liu, Yakui Deng and Bin Ni for funding their PhD scholarships.

Received: ((will be filled in by the editorial staff))
Revised: ((will be filled in by the editorial staff))
Published online: ((will be filled in by the editorial staff))

References

[1] X. Xia, C. M. Spadaccini, J. R. Greer, *Nat. Rev. Mater.* **2022**, *7*, 683.
[2] P. -G. de Gennes, *CR Acad. Sci. Paris, Ser. B* **1975**, *281*, 101.
[3] M. Hébert, R. Kant R, P. -G. de Gennes, *J. Phys. I* **1997**, *7*, 909.
[4] M. H. Li, P. Keller, *Phil. Trans.R. Soc. A* **2006**, *364*, 2763.
[5] C. Ohm, M. Brehmer, R. Zentel, *Adv. Mater.* **2010**, *22*, 3366.
[6] T. J. White, D. J. Broer, *Nat. Mater.* **2015**, *14*, 1087.
[7] S. W. Ula, N. A. Traugutt, R. H. Volpe, R. R. Patel, K. Yu, C. M. Yakacki, *Liq. Cryst. Rev.* **2018**, *6*, 78.

[8] M. H. Li, P. Keller, J. Yang, P. A. Albouy, *Adv. Mater.* **2004**, *16*, 1922.

[9] J. Küpfer, H. Finkelmann, *Makromol. Chem., Rapid Commun.* **1991**, *12*, 717.

[10] D. L. Thomsen III, P. Keller, J. Naciri, R. Pink, H. Jeon, D. Shenoy, B. R. Ratna, *Macromolecules* **2001**, *34*, 5868

[11] T. H. Ware, M. E. McConney, J. J. Wie, V. P. Tondiglia, T. J. White, *Science* **2015,** *347*, 982

[12] C. M. Yakacki, M. Saed, D. P. Nair, T. Gong, S. M. Reed, C. N. Bowman, *RSC Adv.* **2015**, *5*, 18997.

[13] T. Ikeda, J. Mamiya, Y. Yu, *Angew. Chem. Int. Ed.* **2007**, *46*, 506.

[14] H. K. Bisoyi, Q. Li, *Chem. Rev.* **2016**, *116*, 15089.

[15] M. H. Li, P. Keller, B. Li, X. Wang, M. Brunet, *Adv. Mater.* **2003**, *15*, 569.

[16] S. Iamsaard, S. J. Asshoff, B. Matt, T. Kudernac, J. J. Cornelissen, S. P. Fletcher, N. Katsonis, *Nat. Chem.* **2014**, *6*, 229.

[17] K. Kumar, C. Knie, D. Bleger, M. A. Peletier, H. Friedrich, S. Hecht, D. J. Broer, M. G. Debije, A. P. Schenning, *Nat. Commun.* **2016**, *7*, 11975.

[18] T. Ube, K. Kawasaki, T. Ikeda, *Adv. Mater.* **2016**, *28*, 8212.

[19] O. M. Wani, H. Zeng, A. Priimagi, *Nat. Commun.* **2017**, *8*, 15546.

[20] A. H. Gelebart, D. J. Mulder, G. Vantomme, A. Schenning, D. J. Broer, *Angew. Chem. Int. Ed.* **2017**, *56*, 13436.

[21] X. Zheng, Y. Jia, A. Chen, *Nat. Commun.* **2021**, *12*, 4875.

[22] W. Lehmann, H. Skupin, C. Tolksdorf, E. Gebhard, R. Zentel, P. Kruger, M. Losche, F. Kremer, *Nature* **2001**, *410*, 447.

[23] H. Finkelmann, M. Shahinpoor, In Smart Structures and Materials: *Electroactive Polymer Actuators and Devices (EAPAD)* **2002**.

[24] A. Agrawal, H. Chen, H. Kim, B. Zhu, O. Adetiba, A. Miranda, A. Cristian Chipara, P. M. Ajayan, J. G. Jacot, R. Verduzco, *ACS Macro Lett.* **2016**, *5*, 1386.

[25] M. Wang, Z. W. Cheng, B. Zuo, X. M. Chen, S. Huang, H. Yang, *ACS Macro Lett.* **2020**, *9*, 860.

[26] H. Kim, J. A. Lee, C. P. Ambulo, H. B. Lee, S. H. Kim, V. V. Naik, C. S. Haines, A. E. Aliev, R. Ovalle-Robles, R. H. Baughman, T. H. Ware, *Adv. Funct. Mater.* **2019**, *29*, 1905063.

[27] S. Schuhladen, F. Preller, R. Rix, S. Petsch, R. Zentel, H. Zappe, *Adv. Mater.* **2014**, *26*, 7247.

[28] C. Wang, K. Sim, J. Chen, H. Kim, Z. Rao, Y. Li, W. Chen, J. Song, R. Verduzco, C. Yu, *Adv. Mater.* **2018**, *30*, e1706695.

[29] Q. He, Z. Wang, Y. Wang, A. Minori, M. T. Tolley, S. Cai, *Sci. Adv.* **2019**, *5*, eaax5746.

[30] J. M. Boothby, J. C. Gagnon, E. McDowell, T. Van Volkenburg, L. Currano, Z. Xia, *Soft Robot.* **2022**, *9*, 154.

[31] T. A. Kent, M. J. Ford, E. J. Markvicka, C. Majidi, *Multifunct. Mater.* **2020**, *3*, 025003.

[32] M. J. Ford, M. Palaniswamy, C. P. Ambulo, T. H. Ware, C. Majidi, *Soft Matter* **2020**, *16*, 5878-5885

[33] J. Sun, Y. Wang, W. Liao, Z. Yang, *Small* **2021**, *17*, e2103700.

[34] F. Greco, V. Domenici, T. Assaf, S. Romiti, V. Mattoli, Bending actuation of a composite liquid crystal elastomer via direct Joule heating. In *2012 4th IEEE RAS & EMBS International Conference on Biomedical Robotics and Biomechatronics (BioRob)* IEEE, **2012**, 646-651.

[35] F. Greco, V. Domenici, S. Romiti, T. Assaf, B. Zupančič, J. Milavec, B. Zalar, B. Mazzolai, V. Mattoli, *Mol. Cryst. Liq. Cryst.* **2013**, *572*, 40.

[36] C. Feng, C. P. H. Rajapaksha, J. M. Cedillo, C. Piedrahita, J. Cao, V. Kaphle, B. Lussem, T. Kyu, A. Jakli, *Macromol. Rapid Commun.* **2019**, *40*, e1900299.

[37] C. P. H. Rajapaksha, M. D. T. Gunathilaka, S. Narute, H. Albehaijan, C. Piedrahita, P. Paudel, C. Feng, B. Lussem, T. Kyu, A. Jakli, *Molecules* **2021**, *26*, 4234.

[38] M. Yao, B. Wu, X. Feng, S. Sun, P. Wu, *Adv. Mater.* **2021**, *33*, e2103755.

[39] M. Zadan, D. K. Patel, A. P. Sabelhaus, J. Liao, A. Wertz, L. Yao, C. Majidi, *Adv. Mater.* **2022**, *34*, e2200857.

[40] J. G. Martinez, C. Plesse, F. Vidal, W. Zheng, in Electromechanically Active Polymers: A Concise Reference, (Ed: F. Carpi), *Springer International Publishing, Cham* **2016**.

[41] K. Rohtlaid, G. T. M. Nguyen, S. Ebrahimi‐Takalloo, T. N. Nguyen, J. D. W. Madden, F. Vidal, C. Plesse, *Adv. Mater. Technol.* **2021**, *6*, 2001063.

[42] K. Rohtlaid, G. T. M. Nguyen, C. Soyer, E. Cattan, F. Vidal, C. Plesse, *Adv. Electron. Mater.* **2019**, *5*, 1800948.

[43] L. Groenendaal, F. Jonas, D. Freitag, H. Pielartzik, J. R. Reynolds, *Adv. Mater.* **2000**, *12*, 481.

[44] Z. Zhao, G. F. Richardson, Q. Meng, S. Zhu, H. C. Kuan, J. Ma, *Nanotechnology* **2016**, *27*, 042001.

[45] Y. Xia, K. Sun, J. Ouyang, *Adv. Mater.* **2012**, *24*, 2436.

[46] H. Okuzaki, S. Takagi, F. Hishiki, R. Tanigawa, *Sens. Actuators B Chem.* **2014**, *194*, 59.

[47] K. Ikushima, S. John, A. Ono, S. Nagamitsu, *Synth. Met.* **2010**, *160*, 1877.

[48] A. Fannir, R. Temmer, G. T. M. Nguyen, L. Cadiergues, E. Laurent, J. D. W. Madden, F. Vidal, C. Plesse, *Adv. Mater. Technol.* **2019**, *4*, 1800519.

[49] M. Deutsch, *Phys. Rev. A* **1991**, *44*, 8264-8270.

[50] Y. Zhong, G. T. M. Nguyen, C. Plesse, F. Vidal, E. W. H. Jager, *J. Mater. Chem. C* **2019**, *7*, 256.

[51] A. Fannir, C. Plesse, G. T. M. Nguyen, F. Vidal, *Smart Mater. Struct.* **2021**, *30*, 025041.

[52] M. Berggren, G. G. Malliaras, *Science* **2019**, *364*, 233.

[53] A. K. Tripathi, *Mater. Today Energy* **2021**, *20*, 100643.

[54] A. Khaldi, C. Plesse, F. Vidal, S. K. Smoukov, *Adv. Mater.* **2015**, *27*, 4418.